Imaging the Temporal Evolution of Molecular Orbitals during Ultrafast Dissociation

H. Sann,[1] T. Havermeier,[1] C. Müller,[1] H.-K. Kim,[1] F. Trinter,[1] M. Waitz,[1] J. Voigtsberger,[1] F. Sturm,[1] T. Bauer,[1]
R. Wallauer,[2] D. Schneider,[1] M. Weller,[1] C. Goihl,[1] J. Tross,[1] K. Cole,[1] J. Wu,[1] M. S. Schöffler,[1] H. Schmidt-Böcking,[1]
T. Jahnke,[1,*] M. Simon,[3] and R. Dörner[1,†]

[1]*Institut für Kernphysik, Universität Frankfurt, Max-von-Laue-Strasse 1, 60438 Frankfurt, Germany*
[2]*Fachbereich Physik, Philipps-Universität Marburg, Renthof 5, 35032 Marburg, Germany*
[3]*Sorbonne Universités, UPMC Université Paris 06, CNRS, UMR 7614, Laboratoire de Chimie Physique-Matière et Rayonnement,
F-75005 Paris, France*

We investigate the temporal evolution of molecular frame angular distributions of Auger electrons emitted during ultrafast dissociation of HCl following a resonant single-photon excitation. The electron emission pattern changes its shape from that of a molecular σ orbital to that of an atomic p state as the system evolves from a molecule into two separated atoms.

The making and breaking of chemical bonds is the heart of every chemical reaction. The essence of this process can be studied already in the transition from two separated atoms into a diatomic molecule or vice versa. The electron density distributions before and after the bond formation process, i.e., the atomic and molecular orbitals, are well known, but tracing the electron density during this process in an experiment is very challenging. This is first because of the short time scales on which these processes occur and second because of the very limited availability of tools that are capable to sense electron densities on an atomic scale. Accordingly, the vast majority of corresponding experimental works in femto- and attochemistry focuses either on the time evolution of *energy eigenvalues* [1] or on the motion of the nuclei instead. In these studies, the spatial evolution of the electron density distribution which makes the bond has to be left to theory. Pioneering experimental work, which was directly sensitive to the temporal evolution of the shape of the electronic orbitals, was reported by Davies *et al.* They employed a conventional pump-probe laser spectroscopy scheme to examine the dissociation of NO_2 into NO and O [2] after valence shell excitation and subsequent photoionization. The time scale in this case was of ~1 ps, and the time resolution of the latter measurement was in the range of 100 fs. This work and several later studies of time-resolved molecular frame and laboratory frame photoelectron angular distributions (see, e.g., [3] or the inverse process of higher harmonic generation [4,5]) demonstrated their sensitivity to orbital structures.

In the present work, we revisit the problem of probing the charge cloud upon the transition from a molecule into separated atoms on an even shorter time scale of a few femtoseconds. A sketch of our experimental strategy is shown in Fig. 1. We excite an electron from an inner shell of a diatomic molecule AB (which is HCl in our case) to the lowest antibonding orbital (AB^*). This establishes the

pump step of our experiment. The potential energy surface of the excited AB^* is steeply repulsive. Thus, after the pump step, the molecule rapidly dissociates into two separated atoms. The time scale for this ultrafast dissociation is—in the case of HCl—a few femtoseconds only [6–8]. In order to access this time scale in our experiment, we make use of an ultrafast intrinsic molecular clock, the ultrafast
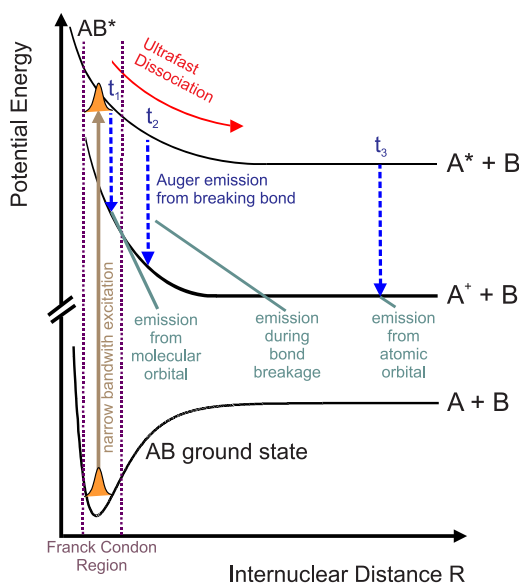

FIG. 1. Sketch of single-photon-induced ultrafast dissociation. A narrow bandwidth single photon excites an electron from an inner shell to an antibonding orbital with a steeply repulsive potential energy curve. Following this pump step, the molecule starts to dissociate. During this dissociation, the Auger electron is emitted, and the internuclear distance at the instance of decay is encoded in the electron energy and the kinetic energy of the fragments. We measure the angular distribution of this electron in the body-fixed molecular frame for different emission times or internuclear distances.

243002-1

dissociation, which is started by the excitation. During the dissociation, the inner shell excited state and an Auger electron are emitted from the dissociating molecule. The Auger lifetime is of the order of the dissociation time, so that the decay can take place either within the molecular Franck-Condon region, during the dissociation when the system is in a transition state between a molecule and two separated atoms, or at larger distances when the molecule is already fragmented into two atoms. For each individual molecule, the internuclear distance at which the decay has occurred is different, but it is encoded in the kinetic energy of the ionic fragments and, as well, the energy of the emitted Auger electron (see Fig. 1). This is different than traditional pump-probe experiments, where the probe step is initiated by the experimentalist at a certain delay time which is then scanned. In our approach, on the contrary, for each molecule the individual delay between the excitation and probe sets itself randomly by the nondeterministic quantum nature of the Auger decay, but it encodes itself in another measured quantity, the kinetic energy of the fragments. By measuring these energies, the internuclear distance and hence (indirectly) the time at which the decay occurred are obtained for each individual decay event.

The individual pieces of this strategy are all well established. Experimental investigations of ultrafast dissociation were pioneered by Morin and Nenner [9], who examined HBr. The HCl case has been studied experimentally and theoretically already several times [7,8,10–19]. In these experiments, the Auger electron energy distribution was measured as a function of the photon energy. The spectra show narrow lines which are independent of the photon energy. The energies of these lines correspond to an atomic decay; i.e., the Auger decay occurred after completion of the dissociation when the atoms were already separated. These atomic lines have a tail towards lower Auger electron energies, which is the fingerprint of a decay at smaller internuclear distances, i.e., before the potential energy curves of the core excited and final state become parallel. More recently, ultrafast dissociation has also been investigated by electron ion coincidence experiments [20,21]

A further well-established piece of our strategy consists of inferring the internuclear distance from measured fragment energies. This is, for example, at the heart of Coulomb explosion imaging. See Ref. [22] for an example taking this to the quantum limit and Ref. [23] for an example in which electron angular distributions are linked to molecular internuclear distances.

The third ingredient to our experimental scheme—using an Auger electron angular distribution in the molecular frame as a fingerprint of the orbital structure—has been first theoretically established in Ref. [24]. Experimentally, this has been shown, e.g., for Auger electrons emitted after K-shell ionization of CO (where σ and π orbitals show vastly different angular distributions) [25] and, as well, in

investigation on N_2 [26] and O_2 [27]. In the present work, we combine all three aforementioned techniques to finally *probe* the orbital evolution during a bond breakage.

A cold target recoil ion momentum spectroscopy reaction microscope was used to conduct the measurements [28–30]. The experiment was performed at the BESSY synchrotron radiation source at beam line UE46 PGM-1 in single bunch operation. Circularly polarized photons of an energy in the region of $h\nu = \sim 200$ eV were focused into a supersonic gas jet, creating Auger electrons of approximately 180 eV kinetic energy. The gas jet was precooled to a temperature of 160 K. This decreases the internal temperature of the jet and accordingly increases the momentum resolution of our measurement. To avoid condensation of the HCl molecules due to the extensive cooling, the gas jet consisted of 95% helium and only 5% HCl. Electrons and ions created in the photoreaction were guided by electric and magnetic fields to two position- and time-sensitive microchannel plate detectors with delay line readout [31]. In order to resolve the different dissociation channels, an electron energy resolution of approximately $1:180$ was needed. To achieve this goal, the electron arm of the spectrometer incorporated a retardation region [30]. On the ion arm (with an overall length of 510 mm), an electrostatic lens was used to improve the momentum resolution [32]. By measuring the electron and the ion momenta in coincidence, the relative emission angle between the two is obtained, yielding the electron emission distribution in the body-fixed frame.

In reality, the situation is considerably more complicated than depicted by the sketch shown in Fig. 1, as there are many more states involved. The relevant potential energy curves for our study in HCl are shown in Fig. 2. We excite the chlorine $2p$ electron to the lowest unoccupied molecular orbital 6σ [Fig. 2(a)]. Because of the spin orbit interaction in the $2p$ shell, two potential energy curves corresponding to a hole of $2p_{1/2}$ and $2p_{3/2}$ character emerge. After the Auger decay and the dissociation, the molecule is fragmented into a neutral H atom and a Cl^+ ion. Depending on which of the $3p$ electrons has been ejected, the final state can be of either ^1S, ^1D, or ^3P symmetry. Measuring the kinetic energy of the Auger electron and the kinetic energy release (KER) of the H and Cl^+ fragments for each event allows us to disentangle the initial excited and final states by means of energy conservation. In our experiment, the energy of the neutral is obtained from the measured momenta of the electron and the Cl^+ using momentum conservation. This leaves us with a subset of measured data belonging only to a decay along the potential energy curves shown in Fig. 2(f), for which the situation is almost as clean as in the sketch shown in Fig. 1. In the following paragraphs, the constraints applied to the total data set in order to choose a decay path of reduced complexity are described in more detail. Figure 2(c) shows the electron energy as a function of the photon energy in the
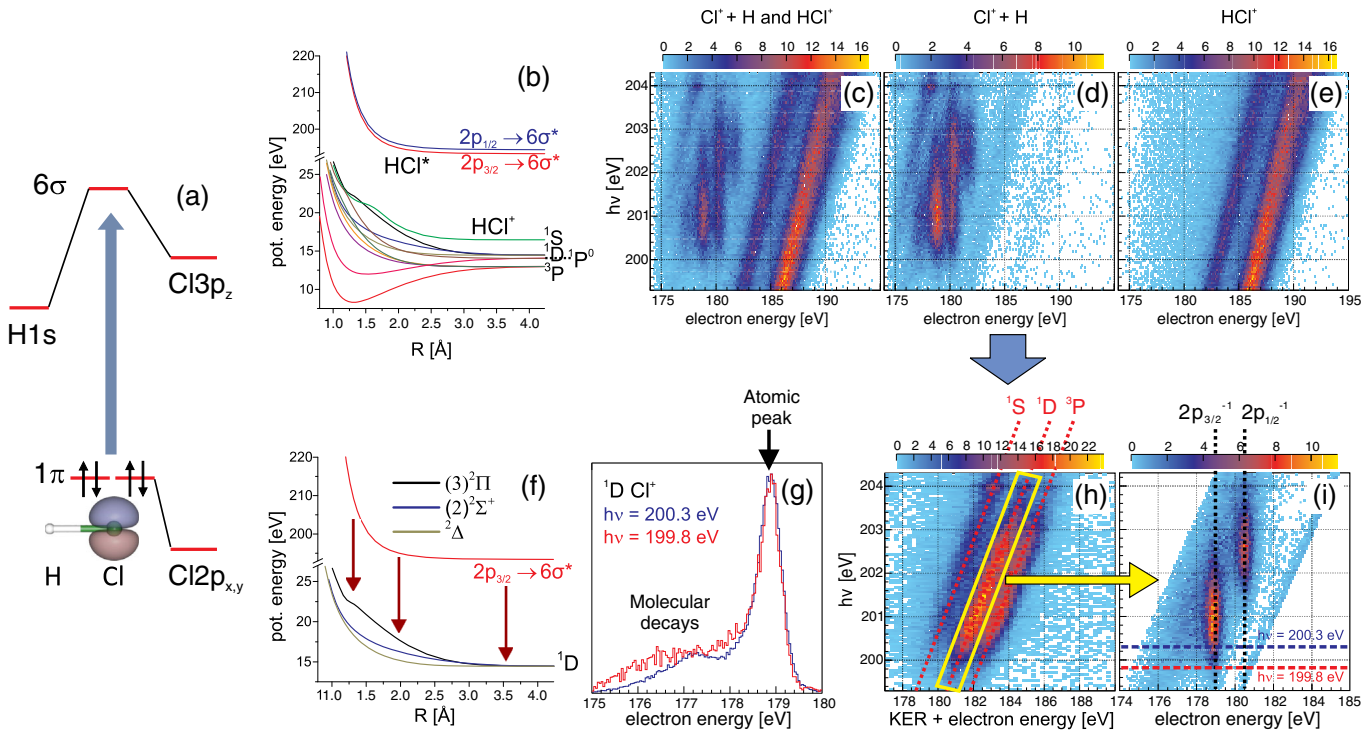
FIG. 2. Ultrafast dissociation of HCl. (a) A 1π electron is excited to the empty 6σ molecular orbital. (b) The corresponding potential energy curves [33,34]. (c) Measured electron energy distributions as a function of the photon energy without a restriction to a certain ionic channel. (d) Subset of data shown in (c) in which a coincident detection of a Cl^+ ion was required. (e) Subset of data shown in (c) which was detected in coincidence with a HCl^+ molecular ion. (f) Subset of potential energy curves depicted in (b), which is relevant for Fig. 3 and panel (g) of this figure. (g) Electron energy distributions for $h\nu = 199.8$ eV and $h\nu = 200.3$ eV and the conditions in panel (i). (h) Sum of the kinetic energy release of $H + Cl^+$ and electron energy versus photon energy. (i) Subset of data in (d) gated on the yellow rectangular area in panel (h).

region of the $2p \rightarrow 6\sigma^*$ excitation integrated over all decay channels available. The data are in agreement with earlier electron spectroscopy work [19] in which the ion was not detected. In this plot, photoelectrons emitted from the valence shell result in diagonal lines, while vertical lines indicate Auger electrons emitted from the dissociating molecule after resonant excitation of the HCl. In this case, the electron energy is independent of the exciting photon energy, and the fragments compensate the missing energy. Splitting the overall data set into two subsets of different ionic final states directly confirms that assignment and shows that the intermediate $6\sigma^*$ state is steeply repulsive: The vertical, atomiclike Auger electron lines are, as expected, always associated with a dissociation into $Cl^+ +$ H as shown in Fig. 2(d). Figures 2(d) and 2(e) show that diagonal features from valence photoelectron emission correspond to a creation of a stable molecular HCl^+ ion. In a next step, we isolate Auger decays which lead to a particular final state of the Cl^+ ion. In Fig. 2(h), the sum kinetic energy of all final state fragments (i.e., electron energy + KER) is plotted versus the photon energy. This histogram shows three diagonal lines corresponding to the ^1S, ^1D, and ^3P final states, respectively. By constraining the measured data set to events associated with dissociation [Fig. 2(d)] and additionally to the subset tagged by the

yellow rectangle in Fig. 2(h), only decays that result in the ^1D final state are examined. Constraining the multidimensional energy distribution thus drastically simplifies the initially congested electron spectrum shown in Fig. 2(c) and reported in Ref. [19], as well, and leaves only two spectral lines which depend differently on the photon energy as shown in Fig. 2(i). These two lines result from the excitation of an electron from either the $2p_{3/2}$ or the $2p_{1/2}$ initial state. In the Franck-Condon region, their excitation threshold differs by approximately 1.5 eV in energy, which leads to the observed difference in the respective resonance energy.

The electron energy distributions obtained at fixed photon energies of 199.8 and 200.3 eV [dashed blue and red lines, respectively, in Fig. 2(i)] are shown in Fig. 2(g). At this energy, only the $2p_{3/2}$ state is excited. The distributions exhibit only a single line at 179 eV with a tail towards lower energies. As described before, the narrow line coincides with the line expected for a decay of an atomic chlorine and corresponds, accordingly, to decays at large distances where the two atoms of the HCl molecule have separated already. The tail towards lower energy results from decays prior to dissociation, i.e., at smaller internuclear distances. The difference in electron energy is compensated by the KER. As shown previously,

the contribution of the molecular decays to the overall distribution increases with the increased detuning of the photon energy from the $2p_{3/2}$ resonance at $h\nu = 200.8$ eV [8,14]. Our clean preparation of a single channel by multicoincidences shows that the molecular part of the electron energy spectrum [Fig. 2(g)] extends to much lower energies than assumed previously. In noncoincident electron spectra, this low energy tail is masked by the contributions from the ^1S states. For this clean subset of the experimental data, we now investigate the electron angular distributions in the molecular frame shown in Fig. 3. The 2D histograms depicted in Figs. 3(a) and 3(f), showing the emission angle of the electron with respect to the momentum vector of the emerging Cl^+ ion and the measured electron kinetic energy for the different photon energies, unveil a strong dependency of the electron angular distribution on the electron energy. The dramatic change of the electron angular distributions is demonstrated in Figs. 3(b)–3(e) and 3(g)–3(j) by investigating different electron energy regions. The lowest electron energy [Figs. 3(b) and 3(g)] corresponds to decays within the molecular region, close to the HCl equilibrium distance. These are the fastest occurring decays; the electron is emitted from a molecular orbital. The corresponding electron angular distribution shows a strong enhancement along the molecular axis in the direction of the H fragment. The emission along the molecular axis is in agreement with the expectation of an electron ejection from a σ orbital (compare, e.g., to Ref. [25]). In the case of slower decays, the molecule stretches prior to the decay. Accordingly, the ion energy (KER) decreases and the electron energy increases. The corresponding electron angular distributions

[Figs. 3(c)–3(e) and 3(h)–3(j)] stepwise lose the prominent feature along the molecular axis. At larger internuclear distances (i.e., for electron energies which correspond to the transition in the separated Cl atom), the angular distribution has taken an opposite shape: It resembles a dipolar distribution oriented perpendicularly to the initial molecular bond. The strong anisotropy occurring in the electron emission from the separated Cl atom is remarkable. The Auger electron angular emission distribution of an unaligned, isolated atom (i.e., from a superposition of $p_{x,y,z}$ states) which was not previously bound in a molecule would be isotropic. For these excited atoms which emerge from the molecular dissociation, on the contrary, the initial molecular axis is still the quantization axis as our data suggest. As shown in Fig. 2(a) and in Ref. [35], the vacancy is mainly created in the $Cl2p_{x,y}$ orbital, where the z axis is given by the molecular axis and the observed dipolar distribution [Figs. 3(d),3(e),3(i), and 3(j)] of the emitted electron coincides with the shape of the atomic $p_{x,y}$ orbital. We find that the angular distributions depend on the energy and thus the internuclear distance but not on the detuning.

In conclusion, we have mapped the evolution of an electronic orbital of the HCl molecule during the breaking of its bond. The shape of the observed electron angular emission pattern shows the transition from a σ-type orbital to an atomic p orbital oriented perpendicularly to the molecular bond. Our method of mapping electron angular distributions during motion in a molecule using narrow bandwidth synchrotron radiation is applicable to many molecules, as ultrafast dissociation has been shown to be a rather general phenomenon occurring in many molecules (see [36,37]). The experimental technique combines the
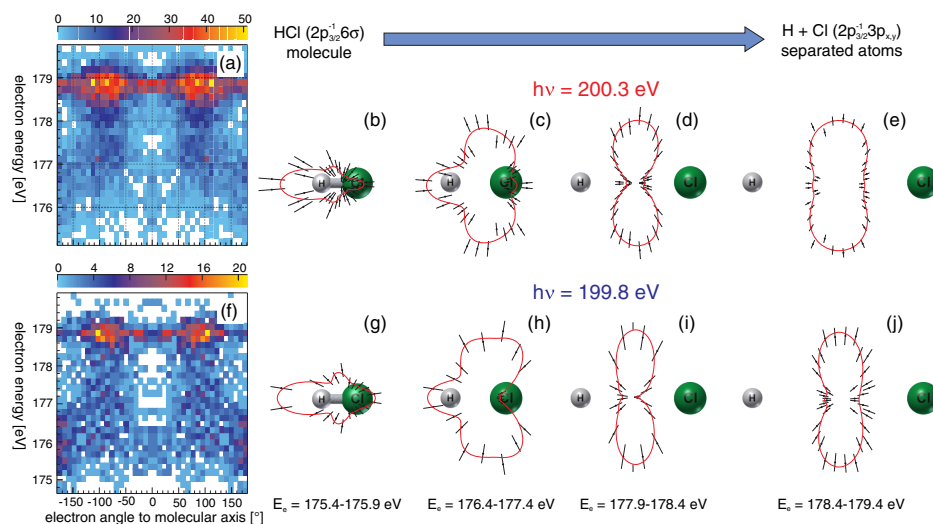

FIG. 3. (a) Electron angular emission distribution with respect to the molecular axis as a function of the electron energy obtained for the decay pathway depicted in Fig. 2(f) recorded at a fixed photon energy of $h\nu = 200.3$ eV. An emission angle of zero corresponds to an emission towards the Cl^+ ion. (b)–(e) Subsets of the data shown in (a) for different regions of electron energy as stated in the figures. The different polar plots correspond to steps in the decay time, i.e., a decay at a time when the molecule is still intact (b) and decays when it has already dissociated [(c),(d)] and the decay occurs in the emitted Cl^* fragment (e). (f)–(j) The same spectra as in (a)–(e) recorded at a fixed photon energy of $h\nu = 199.8$ eV.

state selectivity given by the high spectral resolution with a time resolution in the femtosecond regime provided by an internal molecular clock. To further develop this technique and extract quantitative information on the shape of the orbitals from the Auger electron angular distributions, further theoretical work is needed.

---

*jahnke@atom.uni-frankfurt.de
†doerner@atom.uni-frankfurt.de

[1] A. H. Zewail, Pure Appl. Chem. **72**, 2219 (2000).

[2] J. A. Davies, R. E. Continetti, D. W. Chandler, and C. C. Hayden, Phys. Rev. Lett. **84**, 5983 (2000).

[3] A. Yasuki, W. Kwanghsi, M. Vincent, and T. Kazuo, J. Phys. B **45**, 194006 (2012).

[4] J. Itatani, J. Levesque, D. Zeidler, H. Niikura, H. Pépin, J. C. Kieffer, P. B. Corkum, and D. M. Villeneuve, Nature (London) **432**, 867 (2004).

[5] O. Smirnova, Y. Mairesse, S. Patchkovskii, N. Dudovich, D. Villeneuve, P. Corkum, and M. Y. Ivanov, Nature (London) **460**, 972 (2009).

[6] O. Travnikova, V. Kimberg, R. Flammini, X.-J. Liu, M. Patanen, C. Nicolas, S. Svensson, and C. Miron, J. Phys. Chem. Lett. **4**, 2361 (2013).

[7] A. Menzel, B. Langer, J. Viefhaus, S. Whitfield, and U. Becker, Chem. Phys. Lett. **258**, 265 (1996).

[8] O. Björneholm, S. Sundin, S. Svensson, R. R. T. Marinho, A. Naves de Brito, F. Gel'mukhanov, and H. Ågren, Phys. Rev. Lett. **79**, 3150 (1997).

[9] P. Morin and I. Nenner, Phys. Rev. Lett. **56**, 1913 (1986).

[10] H. Aksela, S. Aksela, M. Ala-Korpela, O.-P. Sairanen, M. Hotokka, G. M. Bancroft, K. H. Tan, and J. Tulkki, Phys. Rev. A **41**, 6000 (1990).

[11] Z. F. Z. Liu, G. M. G. Bancroft, K. H. Tan, and M. Schachter, Phys. Rev. A **48**, R4019 (1993).

[12] E. Kukk, H. Aksela, O.-P. Sairanen, S. Aksela, A. Kivimaki, E. Nommiste, A. Ausmees, A. Kikas, S. J. Osborne, and S. Svensson, J. Chem. Phys. **104**, 4475 (1996).

[13] A. Kivimäki, E. Kukk, J. Karvonen, J. Mursu, E. Nõmmiste, H. Aksela, and S. Aksela, Phys. Rev. A **57**, 2724 (1998).

[14] E. Kukk, A. Wills, N. Berrah, B. Langer, J. D. Bozek, O. Nayadin, M. Alsherhi, A. Farhat, and D. Cubaynes, Phys. Rev. A **57**, R1485 (1998).

[15] R. Feifel, F. Burmeister, P. Sałek, M. N. Piancastelli, M. Bässler, S. L. Sorensen, C. Miron, H. Wang, I. Hjelte, O. Björneholm, A. Naves de Brito, F. K. Gel'mukhanov, H. Agren, and S. Svensson, Phys. Rev. Lett. **85**, 3133 (2000).

[16] S. Sorensen and S. Svensson, J. Electron Spectrosc. Relat. Phenom. **114–116**, 1 (2001).

[17] E. Kukk, J. Electron Spectrosc. Relat. Phenom. **127**, 43 (2002).

[18] W. C. Stolte, R. Guillemin, S.-W. Yu, and D. W. Lindle, J. Phys. B **41**, 145102 (2008).

[19] E. Sokell, A. A. Wills, M. Wiedenhoeft, X. Feng, D. Rolles, and N. Berrah, J. Phys. B **38**, 1535 (2005).

[20] G. Prümper, Y. Tamenori, A. de Fanis, U. Hergenhahn, M. Kitajima, M. Hishino, H. Tanaka, and K. Ueda, J. Phys. B **38**, 1 (2005).

[21] C. Miron and P. Morin, Nucl. Instrum. Methods Phys. Res., Sect. A **601**, 66 (2009).

[22] L. P. Schmidt, T. Jahnke, A. Czasch, M. Schöffler, H. Schmidt-Böcking, and R. Dörner, Phys. Rev. Lett. **108**, 073202 (2012).

[23] N. A. Cherepkov, S. K. Semenov, M. S. Schöffler, J. Titze, N. Petridis, T. Jahnke, K. Cole, L. P. H. Schmidt, A. Czasch, D. Akoury, O. Jagutzki, J. B. Williams, T. Osipov, S. Lee, M. H. Prior, A. Belkacem, A. L. Landers, H. Schmidt-Böcking, R. Dörner, and T. Weber, Phys. Rev. A **82**, 023420 (2010).

[24] K. Zähringer, H.-D. Meyer, and L. S. Cederbaum, Phys. Rev. A **46**, 5643 (1992).

[25] T. Weber, M. Weckenbrock, M. Balser, L. Schmidt, O. Jagutzki, W. Arnold, O. Hohn, M. Schöffler, E. Arenholz, T. Young, T. Osipov, L. Foucar, A. DeFanis, R. DiezMuino, H. Schmidt-Böcking, C. L. Cocke, M. H. Prior, and R. Dörner, Phys. Rev. Lett. **90**, 153003 (2003).

[26] S. K. Semenov, M. S. Schöffler, J. Titze, N. Petridis, T. Jahnke, K. Cole, L. P. H. Schmidt, A. Czasch, D. Akoury, O. Jagutzki, J. B. Williams, T. Osipov, S. Lee, M. H. Prior, A. Belkacem, A. L. Landers, H. Schmidt-Böcking, T. Weber, N. A. Cherepkov, and R. Dörner, Phys. Rev. A **81**, 043426 (2010).

[27] X. J. Liu, Q. Miao, F. Gelmukhanov, M. Patanen, O. Travnikova, C. Nicolas, H. Agren, K. Ueda, and C. Miron, Nat. Photonics **9**, 120 (2015).

[28] R. Dörner, V. Mergel, O. Jagutzki, L. Spielberger, J. Ullrich, R. Moshammer, and H. Schmidt-Böcking, Phys. Rep. **330**, 95 (2000).

[29] J. Ullrich, R. Moshammer, A. Dorn, R. Dörner, L. P. Schmidt, and H. Schmidt-Böcking, Rep. Prog. Phys. **66**, 1463 (2003).

[30] T. Jahnke, T. Weber, T. Osipov, A. Landers, O. Jagutzki, L. Schmidt, C. Cocke, M. Prior, H. Schmidt-Böcking, and R. Dörner, J. Electron Spectrosc. Relat. Phenom. **141**, 229 (2004).

[31] O. Jagutzki, A. Cerezo, A. Czasch, R. Dorner, M. Hattas, V. Mergel, U. Spillmann, K. Ullmann-Pfleger, T. Weber, H. Schmidt-Bocking, and G. Smith, IEEE Trans. Nucl. Sci. **49**, 2477 (2002).

[32] M. S. Schöffler, T. Jahnke, J. Titze, N. Petridis, K. Cole, L. Ph H Schmidt, A. Czasch, O. Jagutzki, J. B. Williams, C. L. Cocke, T. Osipov, S. Lee, M. H. Prior, A. Belkacem, A. L. Landers, H. Schmidt-Böcking, R. Dörner, and T. Weber, New J. Phys. **13**, 095013 (2011).

[33] A. D. Pradhan, K. P. Kirby, and A. Dalgarno, J. Chem. Phys. **95**, 9009 (1991).

[34] S. Carniato, R. Taïeb, R. Guillemin, L. Journel, M. Simon, and F. Gel'mukhanov, Chem. Phys. Lett. **439**, 402 (2007).

[35] S. Carniato, R. Guillemin, W. C. Stolte, L. Journel, R. Taïeb, D. W. Lindle, and M. Simon, Phys. Rev. A **80**, 032513 (2009).

[36] K. Ueda, J. Phys. B **36**, R1 (2003).

[37] P. Morin and C. Miron, J. Electron Spectrosc. Relat. Phenom. **185**, 259 (2012).